

## ***Supporting Information for***

# **Enhanced Stability of $\text{Nb}_3\text{O}_4^-$ and $\text{NbO}^+$ Clusters: The $nxc\pi$ Rule versus Superatomic Nature**

*Yifan Gao,<sup>†</sup> Xin Lei,<sup>†</sup> Ran Cheng,<sup>†</sup> Shiquan Lin,<sup>†</sup> and Zhixun Luo<sup>†,‡,\*</sup>*

<sup>†</sup>State Key Laboratory for Structural Chemistry of Unstable and Stable Species, Institute of Chemistry, Chinese Academy of Sciences, Beijing 100190;

<sup>‡</sup> University of Chinese Academy of Sciences, Beijing 100049, China.

\*Corresponding author. E-mail: [zxluo@iccas.ac.cn](mailto:zxluo@iccas.ac.cn)

## **Contents**

1. Methods.....	2
1.1 Experimental.....	2
1.2 Computational .....	2
2. Experimental details .....	3
3. Benchmark.....	5
2. Structural determination .....	7
4. AdNDP Analysis.....	14
5. Aromaticity .....	15
6. DOS, ELF and CDA analysis .....	17
References .....	20

# 1. Methods

## 1.1 Experimental

A customized MagS source was utilized to produce pure niobium (Nb) clusters. These clusters were then introduced into a flow tube reactor (with a diameter of 60 mm and a length of 1 meter) using high-purity helium gas (purity > 99.999%). Inside the reactor, the clusters reacted with specific reactant gases. The flow rate of the reactant gases was controlled using a gas flowmeter throughout the experiment. To ensure sufficient collisional interactions of the Nb<sup>n</sup> + clusters, the pressure within the flow tube was maintained at approximately 2.6 Torr. This was achieved by using a laminar flow of helium buffer gas from the upstream MagS source and a downstream Roots pump with a high pumping speed of 490 liters per second. After the reaction, the resulting products were transferred into a vacuum system equipped with a differentially pumped ion guide. Finally, the products were analyzed using the self-developed triple quadrupole mass spectrometry (TQMS) equipment.<sup>1</sup>

The niobium cluster anions were also subjected to experiments in a reflection time-of-flight mass spectrometer (Re-TOFMS)<sup>2</sup> that had a custom-made LaVa source and a flow tube with an inner diameter of 6 mm and a length of 60 mm. Metal clusters were generated by sputtering a niobium disk target ( $\Phi = 1.5$  cm, 99.99% purity) using a focused 532-nm laser (Nd:YAG) with a repetition frequency of 10 Hz and a laser pulse energy of 15-20 mJ. The carrier gas employed was He with a purity of 99.999% and a pressure of 1.0 MPa. The carrier gas was high-purity helium (99.999%) at a pressure of 1.0 MPa, which was regulated using a pulsed valve (Parker, Series 9). Another pulsed valve was used to introduce the reaction gas into the system, allowing it to interact with the metal clusters further down the reaction tube. The amount of reaction gas was controlled by adjusting the duration of the pulsed valve. The molecular beam was then directed into the detection chamber through a small-diameter skimmer (diameter = 2 mm) and analyzed by the Re-TOFMS. The signals were recorded using a digital oscilloscope (Teledyne LeCroy HDO6000) by averaging 1000 individual mass spectra, which were saved for further analysis.

## 1.2 Computational

The initial structures of the niobium clusters were designed by examining the experimental and theoretical studies that had been previously reported in the literature, while also considering the variations in spin multiplicity and geometric structure. The Gaussian program<sup>3</sup> was employed to conduct the structural optimization and energetics calculations at the M06L/SDD level of theory. The energies were corrected by zero-point vibrations, and all the calculated isomers were verified to verify that there was no imaginary frequency.

## 2. Experimental details

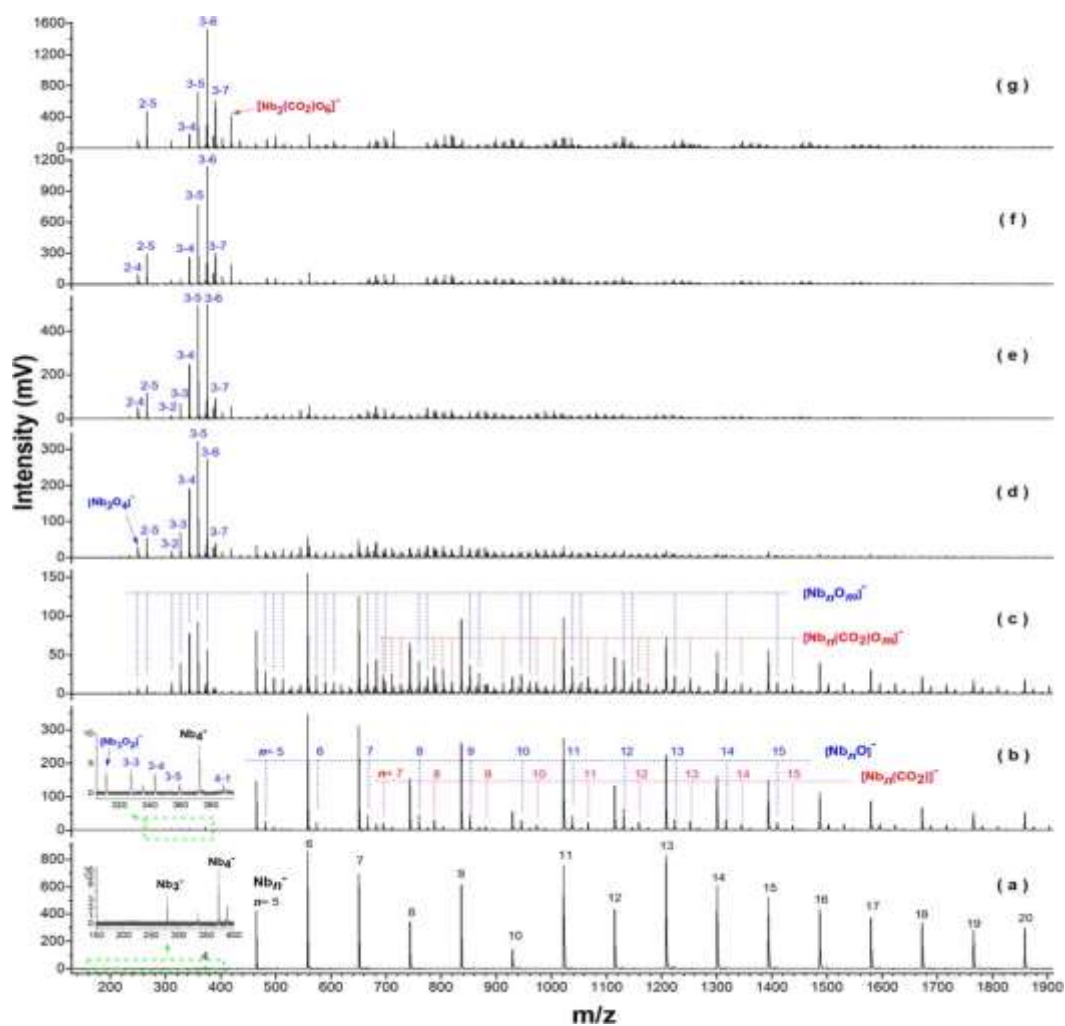


**Fig. S1** Repeated experiments showing the mass spectra of the  $\text{Nb}_n^-$  clusters before and after reacting with  $\text{CO}_2$  (20% in helium), with on-time of the pulse valve at 80, 120, 160, 190, 200, 220  $\mu\text{s}$  respectively.

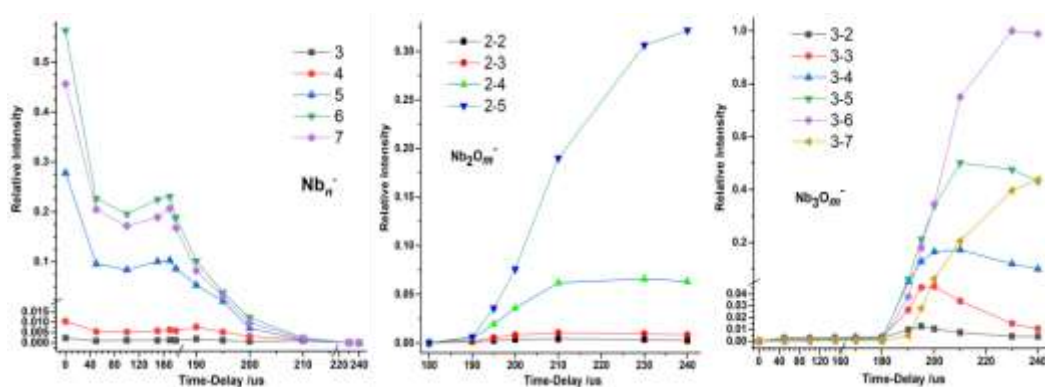


**Fig. S2** Mass abundances of the  $\text{Nb}_n^-$  clusters before and after reacting with  $\text{CO}_2$ .

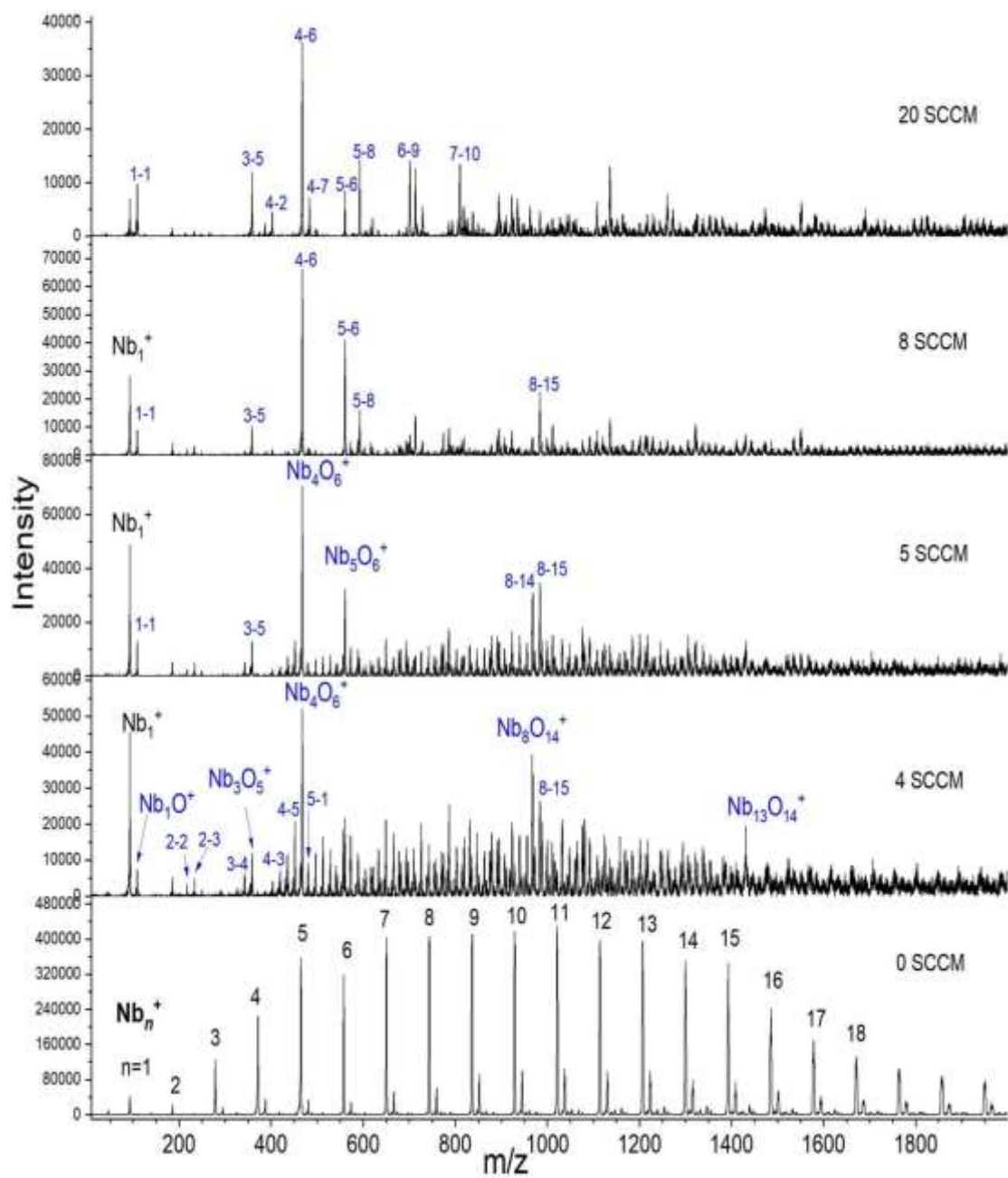


**Fig. S3** Repeated experiments showing the mass spectra of the Nb<sub>n</sub><sup>+</sup> cationic clusters before and after reacting with CO<sub>2</sub> (20% in helium).

### 3. Benchmark

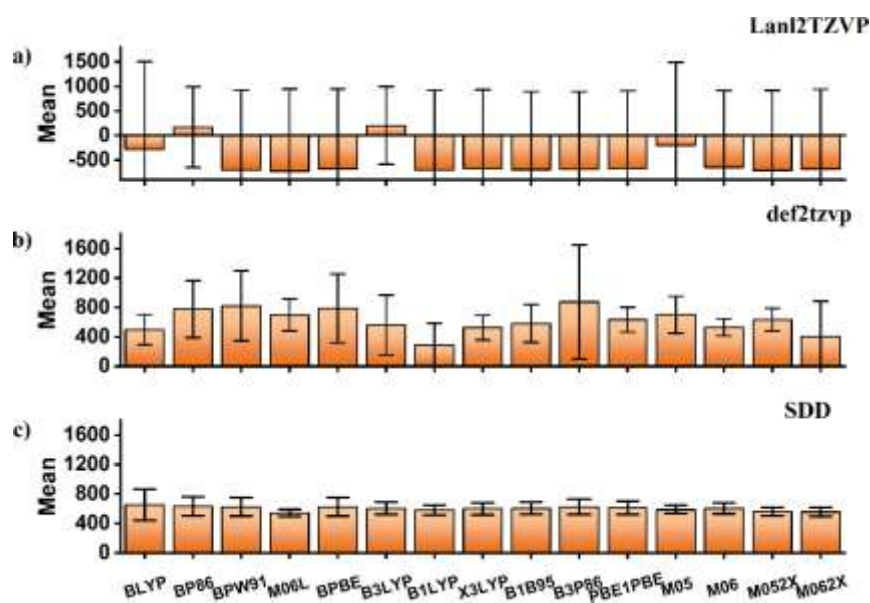


**Fig. S4** a) Variance of functional tests under Lanl2TZVP basis set. b) Variance of functional tests under def2tzvp basis set. c) Variance of functional tests under SDD basis set.

**Table S1** Calculated Nb<sub>2</sub> bond energies and Nb<sub>2</sub><sup>+</sup> bond energies for different functionals under def2tzvp basis set

Basic group	Functional	Nb-Nb(kj/mol)	Nb <sup>+</sup> -Nb (kj/mol)
		513	576.8 ± 9.6
def2tzvp	BLYP	692.0739235	207.803074
	BP86	668.011216	1346.445667
	BPW91	667.8983195	1525.945851
	M06L	699.6668695	999.4412085
	BPBE	568.410248	1486.195781
	B3LYP	79.741686	1073.624711
	B1LYP	62.261107	-3.2845005
	X3LYP	705.130535	303.6259475
	B1B95	927.8963335	308.2730825
	B3P86	375.0920575	2031.945339
	PBE1PBE	885.3789865	561.426418
	M05	1066.680264	650.75643
	M06	379.7076865	644.077158
	M052X	860.0534135	583.8665665
	M062X	816.3808465	-283.3990955

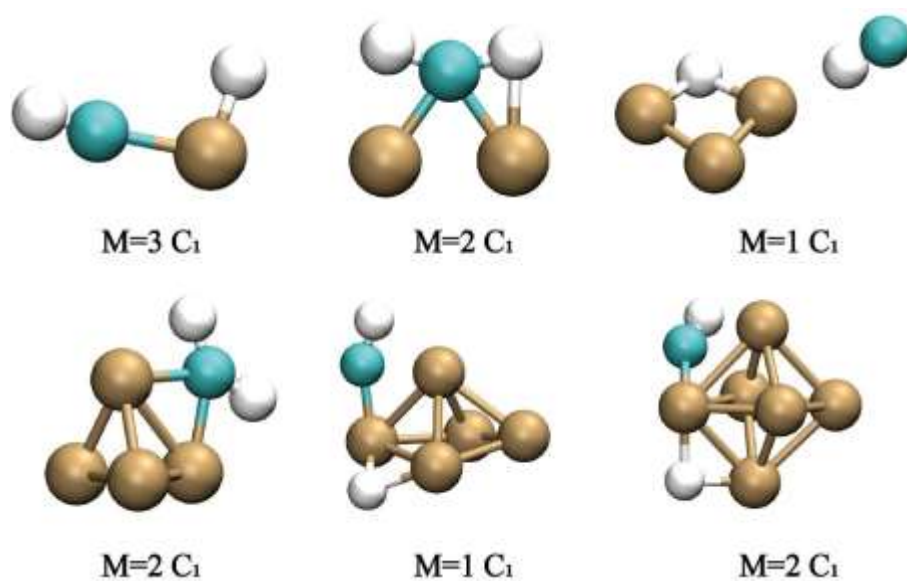
**Table S2** Calculated Nb<sub>2</sub> bond energies and Nb<sub>2</sub><sup>+</sup> bond energies for different functionals under Lan2TZ(f) basis set

Basic group	Functional	Nb-Nb(kj/mol)	Nb <sup>+</sup> -Nb (kj/mol)
		513	576.8 ± 9.6
Lan12TZ(f)	BLYP	-2953.482711	743.100516
	BP86	646.576634	-1058.81164
	BPW91	-2883.507885	-1023.144222
	M06L	-2977.085956	-1008.617331
	BPBE	-2874.678329	-921.188181
	B3LYP	697.983924	-975.2551025
	B1LYP	-2871.753521	-1024.139287
	X3LYP	-2834.143234	-939.0337045
	B1B95	-2781.887907	-1084.462775
	B3P86	-2773.628085	-1069.633951
	PBE1PBE	-2760.63711	-996.823585
	M05	-2729.559067	836.6076985
	M06	-2742.949117	-937.340257
	M052X	-2871.979315	-1045.888929
	M062X	-2875.208679	-929.7079285

**Table S3** Calculated Nb<sub>2</sub> bond energies and Nb<sub>2</sub><sup>+</sup> bond energies for different functionals under SDD basis set

Basic group	Functional	Nb-Nb(kj/mol)	Nb <sup>+</sup> -Nb (kj/mol)
		513	576.8 ± 9.6
SDD	BLYP	560.3473375	970.0093535
	BP86	621.7157745	815.1468615
	BPW91	605.4534275	800.740743
	M06L	492.2103615	591.519899
	BPBE	608.438621	804.5765985
	B3LYP	610.470758	712.392668
	B1LYP	568.9484755	674.301914
	X3LYP	604.4609885	708.701215
	B1B95	628.486939	710.087479
	B3P86	656.2621035	753.57101
	PBE1PBE	629.1144335	731.154491
	M05	616.672189	642.732902
	M06	651.817132	680.3116835
	M052X	521.965153	631.6769215
	M062X	504.51608	631.7346825

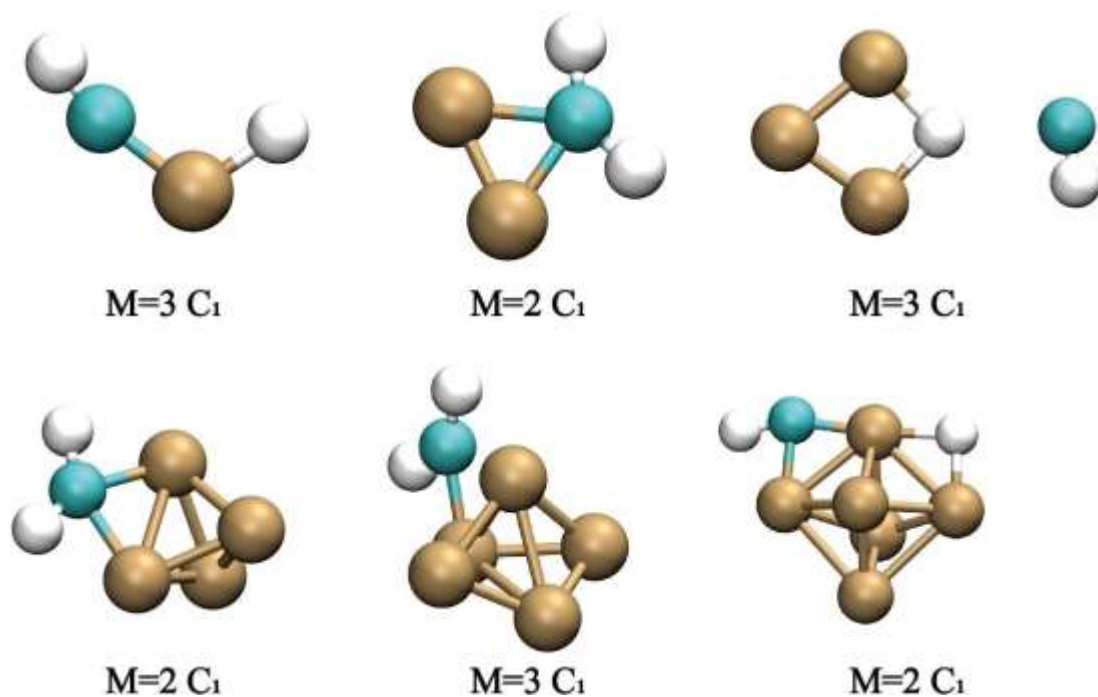
## 2. Structural determination



**Fig. S5** The geometry of  $Nb_nCO_2^+$  ( $n=0-6$ ) clusters. M represents the multiplicity.

**Table S4** Calculated M-O bond length and the M-C bond length of  $Nb_nCO_2^+$  ( $n=0-6$ )

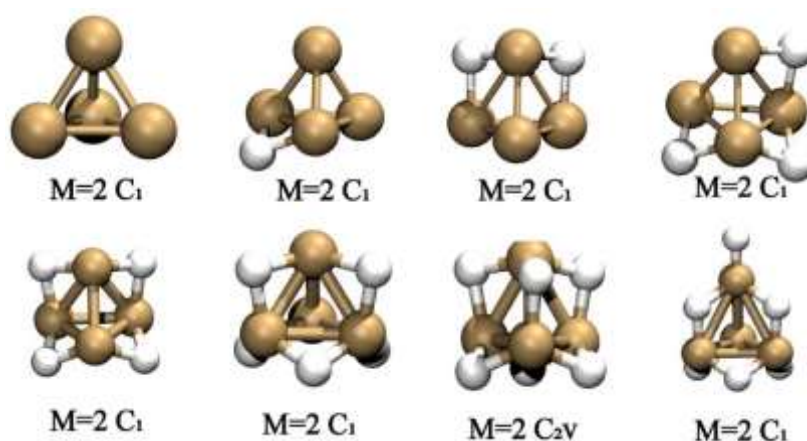
$Nb_nCO_2^+$ ( $n=1-6$ )			
n	$\Delta H/(eV)$	M-O bond length (Å)	M-C bond length (Å)
1	-4.760727716	1.70	2.20
2	-2.542541418	2.07	2.12
3	-3.786573916	1.92	3.44
4	-0.499457905	2.25	2.24
5	-3.833186359	1.92	2.1
6	-4.917272599	1.96	2.03



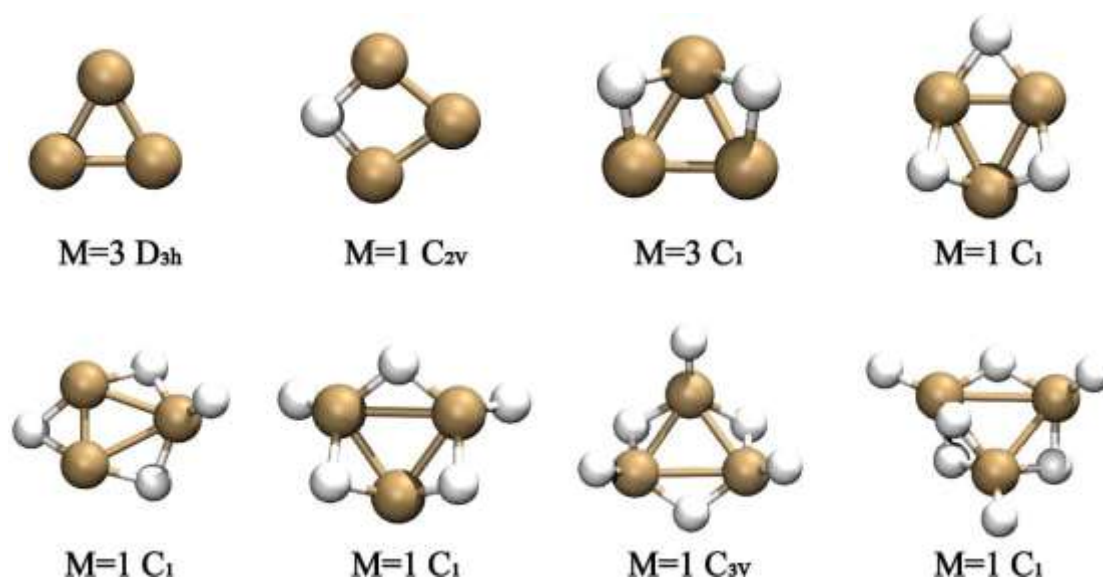
**Fig. S6** The geometry of  $\text{Nb}_n\text{CO}_2^-$  ( $n=0-6$ ) clusters. M represents the multiplicity.

**Table S5** Calculated M-O bond length and the M-C bond length of  $\text{Nb}_n\text{CO}_2^-$  ( $n=1-6$ )

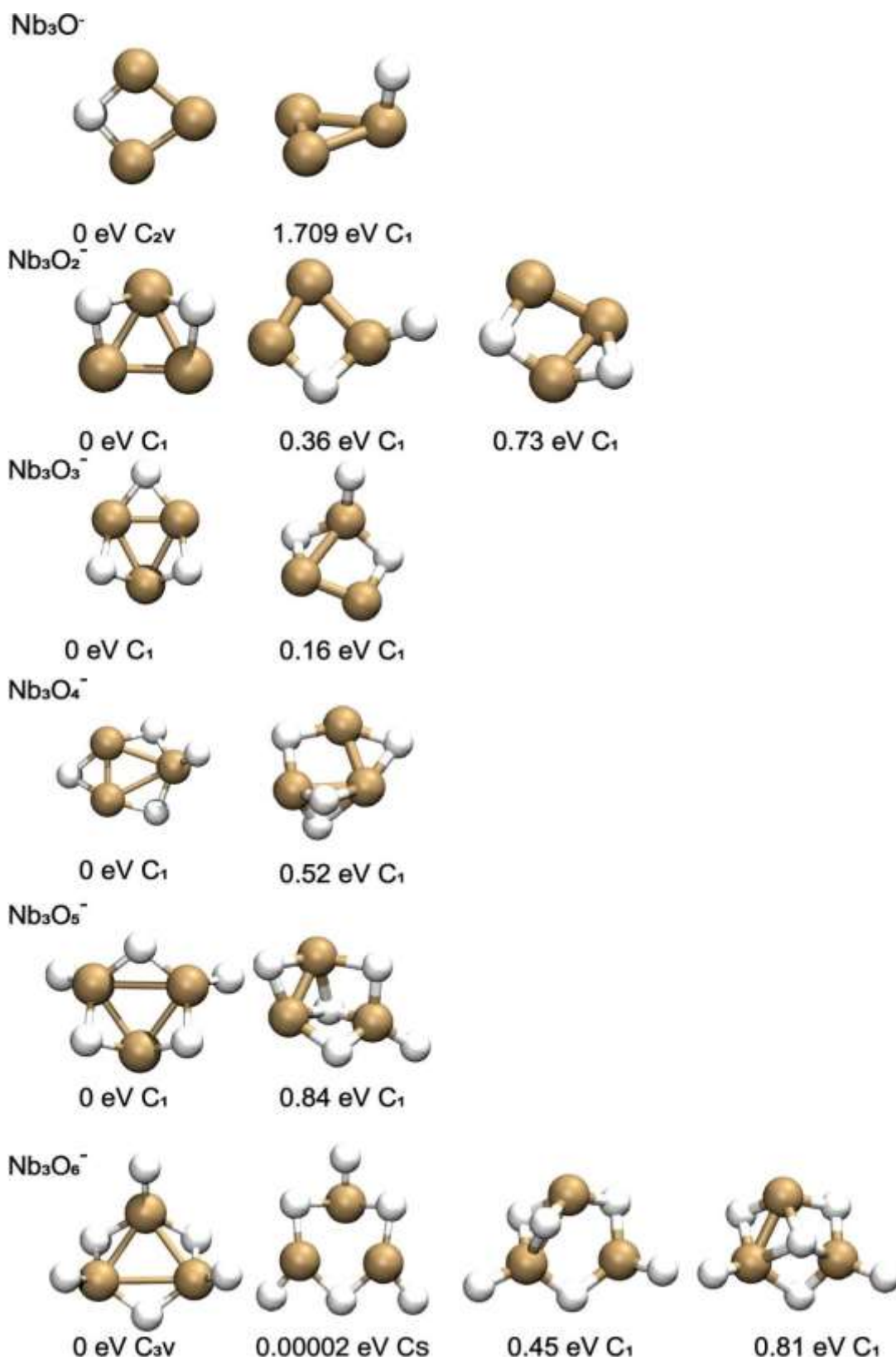
$\text{Nb}_n\text{CO}_2^-$ ( $n=1-6$ )			
n	$\Delta H/(\text{eV})$	M-O bond length (Å)	M-C bond length (Å)
1	-6.599320564	1.77	2.01
2	-2.427466099	2.39	2.18
3	-2.125913797	1.96	4.28
4	-2.909372909	2.32	2.24
5	-2.913454559	2.31	2.21
6	-5.66723497	1.93	2.08



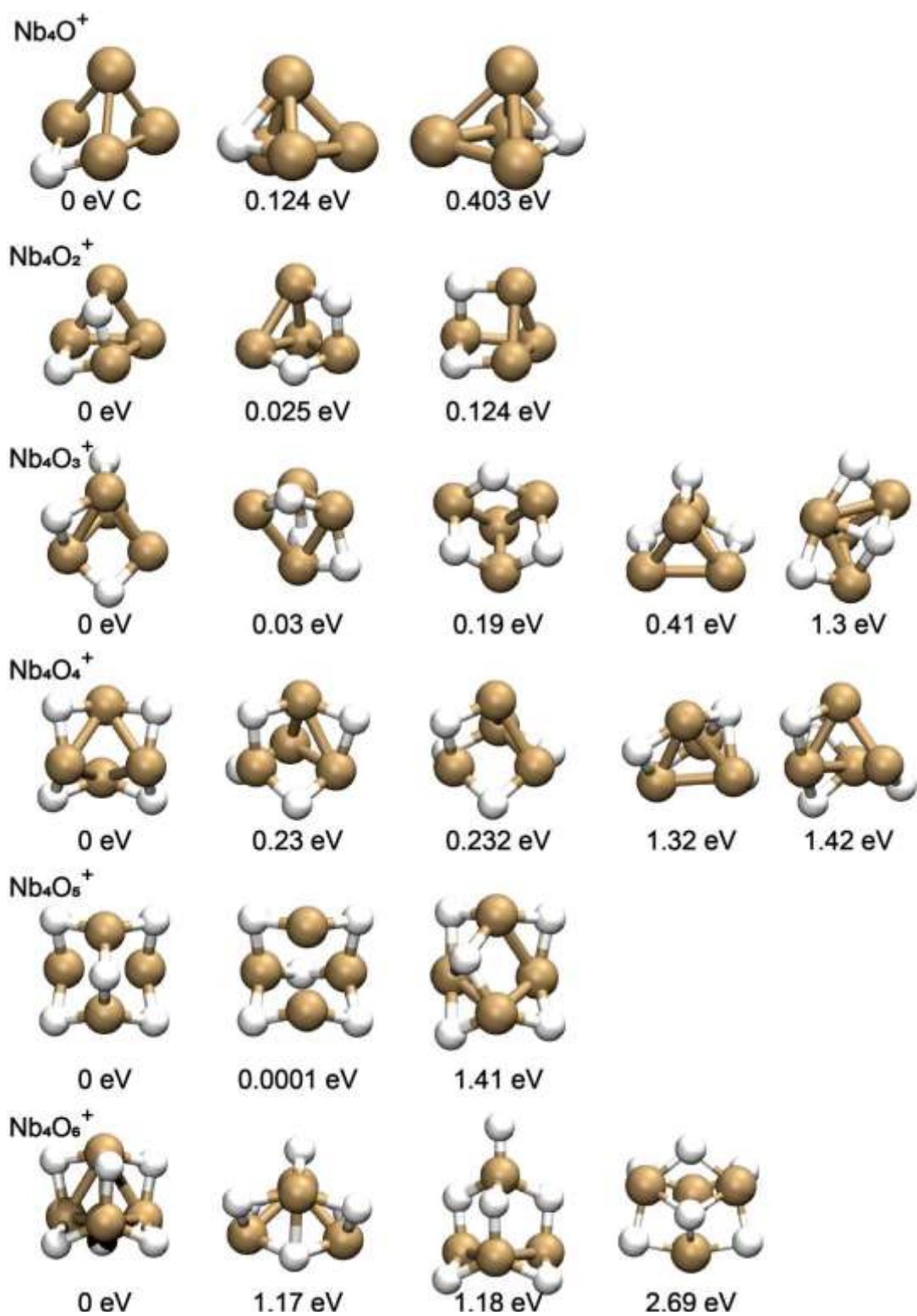
**Fig. S7** The lowest energy structure of  $\text{Nb}_3\text{O}_x^+$  ( $x = 0-7$ ) clusters at the M06L/SDD calculation level, M represents the multiplicity.



**Fig. S8** The lowest energy structure of  $\text{Nb}_3\text{O}_x^-$  ( $x = 0-7$ ) clusters at the M06L/SDD calculation level, M represents the multiplicity.

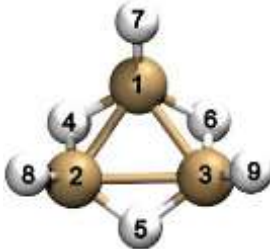


**Fig. S9** The isomers structure of  $\text{Nb}_3\text{O}_x^-$  ( $x = 1-6$ ) clusters optimized at the M06L/SDD level of theory, with energies relative to that of the lowest energy structure.

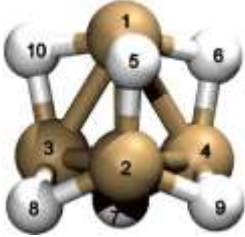


**Fig. S10** The isomers structure of  $\text{Nb}_4\text{O}_x^+$  ( $x = 1-6$ ) clusters optimized at the M06L/SDD level of theory, with energies relative to that of the lowest energy structure.

**Table S6** The calculated bond length and Wiberg bond order of Nb<sub>3</sub>O<sub>6</sub><sup>-</sup>

	Atomic number	Bond length (Å)	Wiberg bond order
	1,7	1.7728	2.52
	3,9	1.7750	2.53
	2,8	1.7749	2.53
	1,4	2.0423	1.11
	1,6	2.0422	1.11
	2,4	1.9539	1.40
	2,5	1.9829	1.26
	3,5	1.9824	1.26
	3,6	1.9544	1.40
	1,2	2.8169	1.10
	1,3	2.8180	1.10
	2,3	3.1905	0.48

**Table S7** The calculated bond length and Wiberg bond order of Nb<sub>4</sub>O<sub>6</sub><sup>+</sup>

	Atomic number	Bond length (Å)	Wiberg bond order
	1,5	2.00	1.16
	1,6	2.00	1.15
	1,10	2.00	1.16
	1,2	2.69	1.02
	1,3	2.69	1.02
	1,4	2.69	1.02
	2,3	2.83	0.78
	2,4	2.83	0.78
	2,9	1.97	1.24
	2,8	1.97	1.25
	3,4	2.83	0.78
	3,7	1.97	1.24
	3,8	1.97	1.25
	4,7	1.97	1.25
	4,9	1.97	1.25

**Table S8** Calculated thermodynamic energy changes of the Nb<sub>4</sub><sup>+</sup> cluster in reacting with CO<sub>2</sub>.

Nb <sub>4</sub> <sup>+</sup> + CO <sub>2</sub> → Nb <sub>4</sub> O <sup>+</sup> + CO	Δ H= -2.14 eV
Nb <sub>4</sub> O <sub>1</sub> <sup>+</sup> + CO <sub>2</sub> → Nb <sub>4</sub> O <sub>2</sub> <sup>+</sup> + CO	Δ H= -2.08 eV
Nb <sub>4</sub> O <sub>2</sub> <sup>+</sup> + CO <sub>2</sub> → Nb <sub>4</sub> O <sub>3</sub> <sup>+</sup> + CO	Δ H= -1.97 eV
Nb <sub>4</sub> O <sub>3</sub> <sup>+</sup> + CO <sub>2</sub> → Nb <sub>4</sub> O <sub>4</sub> <sup>+</sup> + CO	Δ H= -2.18 eV
Nb <sub>4</sub> O <sub>4</sub> <sup>+</sup> + CO <sub>2</sub> → Nb <sub>4</sub> O <sub>5</sub> <sup>+</sup> + CO	Δ H= -2.11 eV
Nb <sub>4</sub> O <sub>5</sub> <sup>+</sup> + CO <sub>2</sub> → Nb <sub>4</sub> O <sub>6</sub> <sup>+</sup> + CO	Δ H= -1.87 eV
Nb <sub>4</sub> O <sub>6</sub> <sup>+</sup> + CO <sub>2</sub> → Nb <sub>4</sub> O <sub>7</sub> <sup>+</sup> + CO	Δ H= -0.06 eV

**Table S9** Calculated thermodynamic energy changes of the Nb<sup>-</sup> cluster in reacting with CO<sub>2</sub>.

Nb <sub>3</sub> <sup>-</sup> + CO <sub>2</sub> → Nb <sub>3</sub> O <sup>-</sup> + CO	Δ H= -2.71 eV
Nb <sub>3</sub> O <sub>1</sub> <sup>-</sup> + CO <sub>2</sub> → Nb <sub>3</sub> O <sub>2</sub> <sup>-</sup> + CO	Δ H= -1.26 eV
Nb <sub>3</sub> O <sub>2</sub> <sup>-</sup> + CO <sub>2</sub> → Nb <sub>3</sub> O <sub>3</sub> <sup>-</sup> + CO	Δ H= -1.98 eV
Nb <sub>3</sub> O <sub>3</sub> <sup>-</sup> + CO <sub>2</sub> → Nb <sub>3</sub> O <sub>4</sub> <sup>-</sup> + CO	Δ H= -2.85 eV
Nb <sub>3</sub> O <sub>4</sub> <sup>-</sup> + CO <sub>2</sub> → Nb <sub>3</sub> O <sub>5</sub> <sup>-</sup> + CO	Δ H= -1.78 eV
Nb <sub>3</sub> O <sub>5</sub> <sup>-</sup> + CO <sub>2</sub> → Nb <sub>3</sub> O <sub>6</sub> <sup>-</sup> + CO	Δ H= -2.32 eV
Nb <sub>3</sub> O <sub>6</sub> <sup>-</sup> + CO <sub>2</sub> → Nb <sub>3</sub> O <sub>7</sub> <sup>-</sup> + CO	Δ H= -1.42 eV

eV

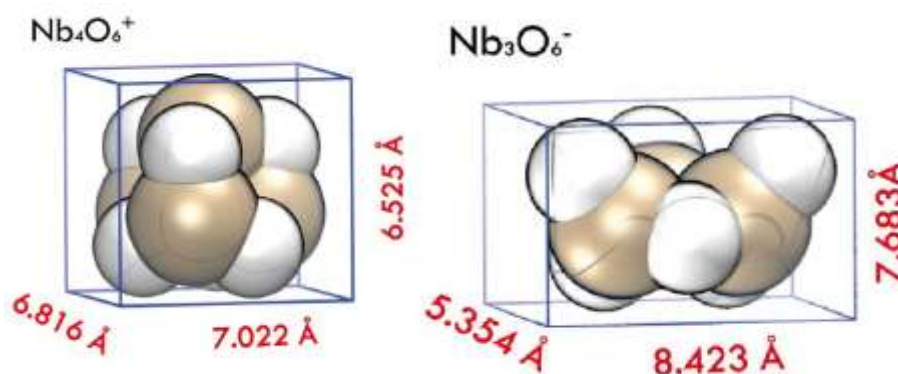


**Fig. S11** The van der waals (VDW) radius of the Nb<sub>4</sub>O<sub>6</sub><sup>+</sup> and Nb<sub>3</sub>O<sub>6</sub><sup>-</sup> clusters.

## 4. AdNDP Analysis

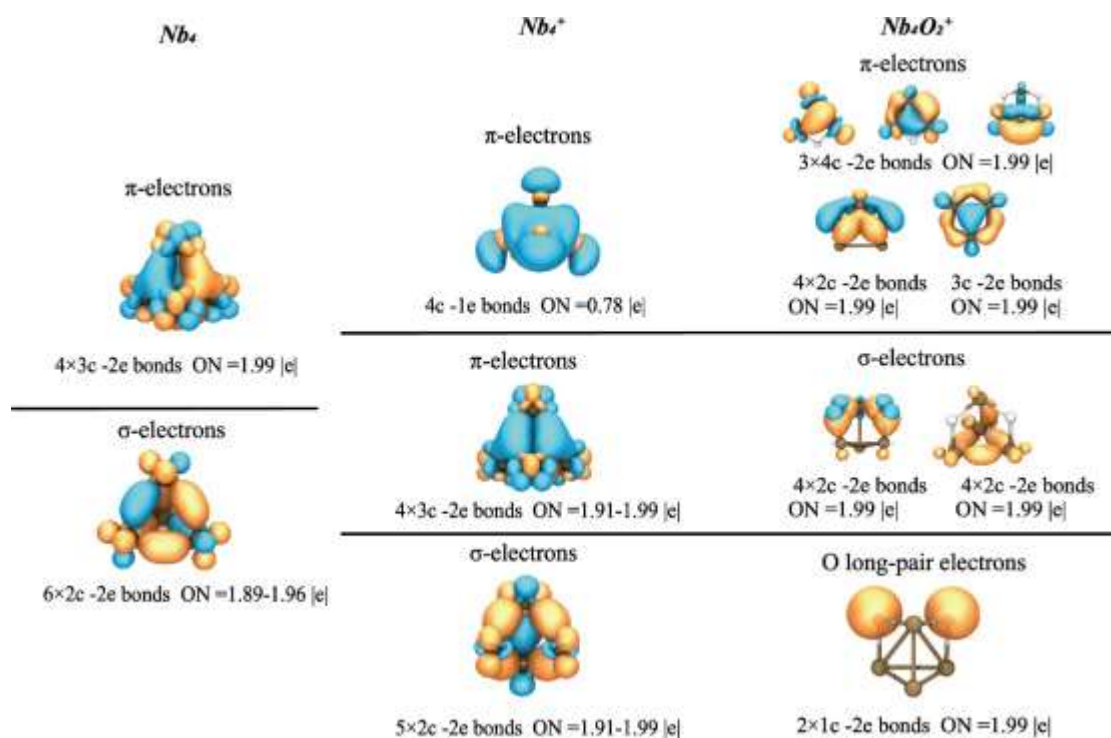


**Fig. S12** AdNDP analysis of (a)  $Nb_4$ , (b)  $Nb_4^+$ , and (c)  $Nb_4O_2^+$ .

According to AdNDP analysis,  $Nb_4$  has a total of 20 valence electrons. The tetrahedron is composed of six 2c-2e bonds that are situated on six edges and four 3c-2e bonds that are situated on four faces. The geometry, electronic structure, and occupancy of  $Nb_4^+$  are all altered by the loss of one electron. The electronic structure is also altered, and one of the metal bonds is elongated. The AdNDP analysis indicates that  $Nb_4^+$  has five 2c-2e-bonds, four 3c-2e-bonds, and one 4c-1e bond, with an occupancy of 0.78. It demonstrates that the electrons that were initially localized on the metal bond begin to delocalize on the metal core following the loss of an electron. The AdNDP analysis of  $Nb_4O_2^+$  and  $Nb_4^+$  revealed that  $Nb_4O_2^+$  contained two lone pairs of (1c-2e, ON= 1.99) localized on the oxygen atom and eight 2c-2e bonds of which four are between Nb-O and four are between Nb-Nb (ON=1.99). Additionally, there is a  $\pi$  bond between the Nb-O atoms (ON=1.99), as well as four 3c-2e-bonds (ON=1.99) between the three Nb elements.

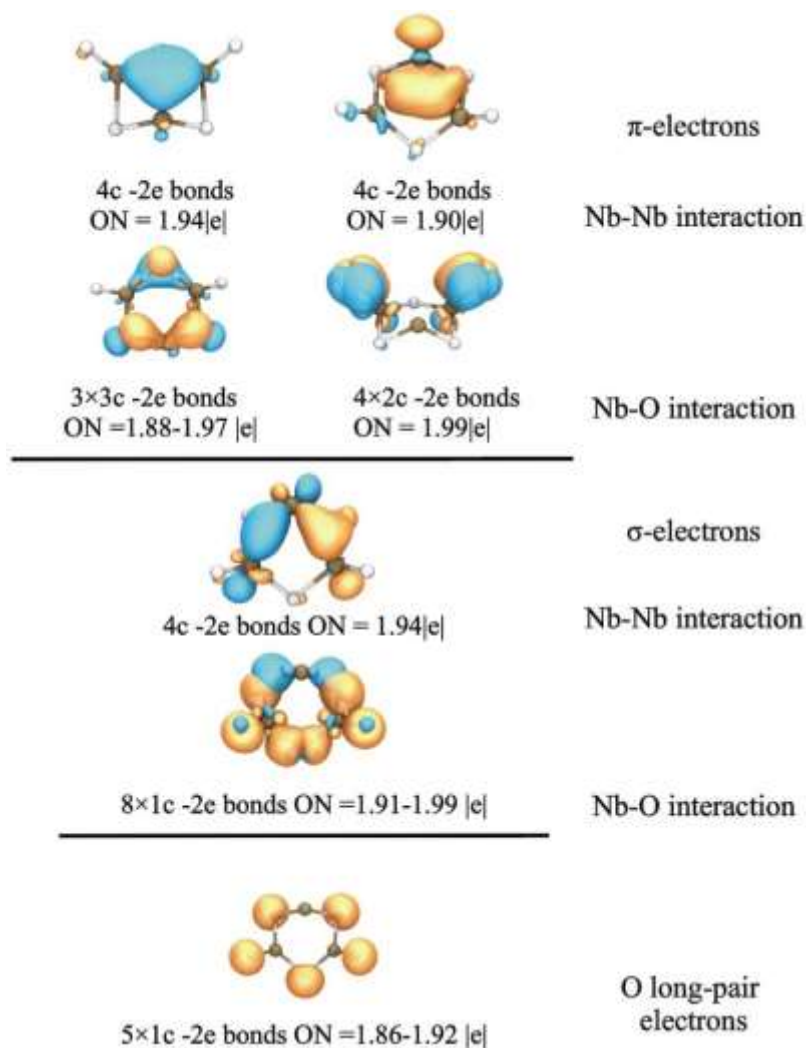


**Fig. S13** AdNDP analysis of the  $\text{Nb}_3\text{O}_5^-$  cluster. The occupation number (ON) is given below each multi-center bond.

## 5. Aromaticity

In order to illustrate the aromaticity of clusters, benzene and  $\text{Pt}_{10}^-$  were chosen as controls. The aromatic characteristic is represented by the value at which the electron is globally delocalized, as demonstrated by the 3D-ELF calculations. According to the findings, the aromatagenity value of benzene was 0.65,  $\text{Nb}_4\text{O}_6^+$  was 0.54, and  $\text{Pt}_{10}^-$  and  $\text{Nb}_3\text{O}_6^-$  were 0.24 and 0.22, respectively. The results suggested that the delocalization of  $\text{Nb}_4\text{O}_6^+$  electrons was more robust than that of  $\text{Pt}_{10}^-$  and  $\text{Nb}_3\text{O}_6^-$ .

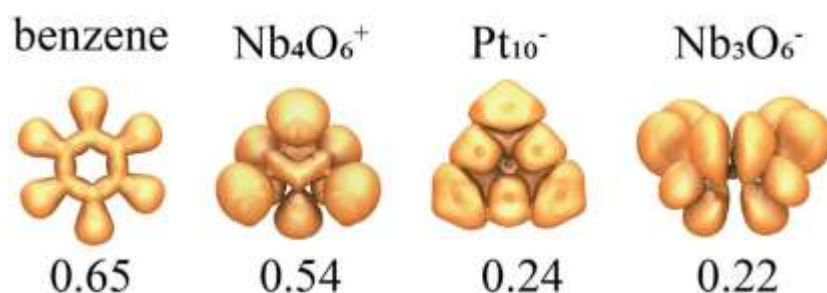


**Fig. S14** Comparison of aromaticity of benzene,  $\text{Nb}_4\text{O}_6^+$ ,  $\text{Pt}_{10}^-$  and  $\text{Nb}_3\text{O}_6^-$ . The values represent iso-surfaces when the  $\pi$ -electron delocalization occurs over the cross-section.



**Fig. S15** The magnetic components of  $\text{Nb}_4\text{O}_6^+$  in different directions

The energy of the overall front-line orbital energy in the process of  $\text{Nb}_4$  becoming  $\text{Nb}_4\text{O}_6^+$  is reduced, which is beneficial for the stability of the metal cluster. Additionally, the addition of oxygen atoms reduces the energy of the S, P and D orbitals of Nb, which is beneficial for the improvement of the relative stability of the cluster. This is demonstrated by superatomic orbital analysis and DOS analysis. The energy of the superatomic S orbital increases and the HOMO-LUMO gap decreases as  $\text{Nb}_4$  becomes  $\text{Nb}_4^+$ . This is conducive to the excitation of electrons, and it is straightforward to react with  $\text{CO}_2$  to produce cluster oxides. The degree of electron delocalization is enhanced by the incorporation of oxygen atoms. The characteristics of superatomic orbitals are also becoming more prominent. The symmetry of  $\text{Nb}_4\text{O}_6^+$  clusters is superior to that of  $\text{Nb}_4\text{O}_2^+$  clusters, and the delocalization of electrons is more uniformly dispersed around the clusters. The characteristic orbitals of superatoms are also more prominent.

## 6. DOS, ELF and CDA analysis

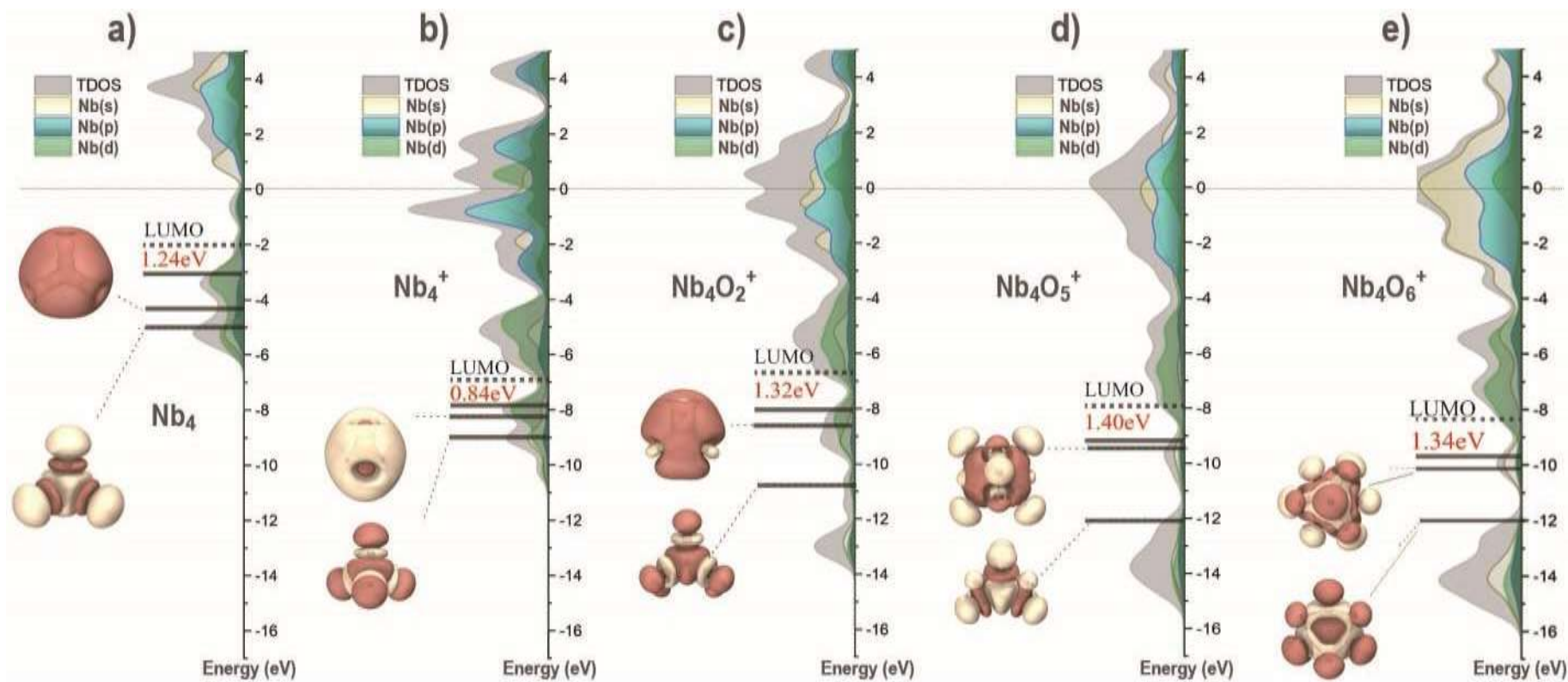


**Fig. S16** A comparison of the superatomic orbitals and DOSs of Nb<sub>4</sub> (a), Nb<sub>4</sub><sup>+</sup> (b), Nb<sub>4</sub>O<sub>2</sub><sup>+</sup> (c), Nb<sub>4</sub>O<sub>5</sub><sup>+</sup> (d), and Nb<sub>4</sub>O<sub>6</sub><sup>+</sup> (e).



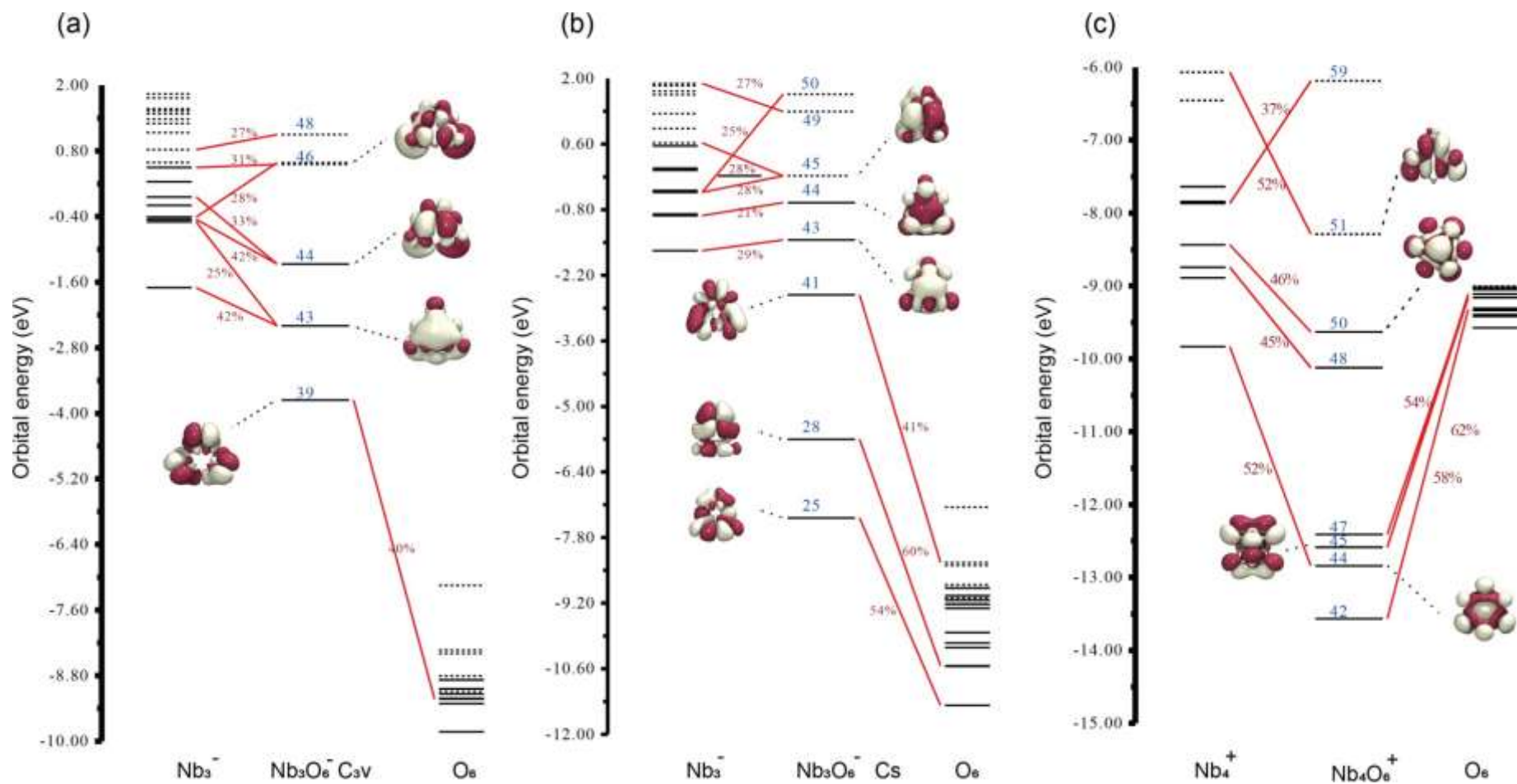


**Fig. S18** Charge decomposition analysis (CDA) of the  $C_{3v}$   $Nb_3O_6^-$  (a),  $C_s$   $Nb_3O_6^-$  (b), and  $Nb_4O_6^+$  clusters.

## References

1. B. Huang, H. Wu, M. Yang and Z. Luo, *Rev. Sci. Instrum.*, 2022, **93**, 113307.
2. H. Zhang, H. Wu, Y. Jia, L. Geng, Z. Luo, H. Fu and J. Yao, *Rev. Sci. Instrum.*, 2019, **90**, 073101.
3. M. J. Frisch, G. W. Trucks, H. B. Schlegel, G. E. Scuseria, M. A. Robb, J. R. Cheeseman, G. Scalmani, V. Barone, G. A. Petersson, H. Nakatsuji, X. Li, M. Caricato, A. V. Marenich, J. Bloino, B. G. Janesko, R. Gomperts, B. Mennucci, H. P. Hratchian, J. V. Ortiz, A. F. Izmaylov, J. L. Sonnenberg, D. Williams-Young, F. Ding, F. Lipparini, F. Egidi, J. Goings, B. Peng, A. Petrone, T. Henderson, D. Ranasinghe, V. G. Zakrzewski, J. Gao, N. Rega, G. Zheng, W. Liang, M. Hada, M. Ehara, K. Toyota, R. Fukuda, J. Hasegawa, M. Ishida, T. Nakajima, Y. Honda, O. Kitao, H. Nakai, T. Vreven, K. Throssell, J. A. Montgomery, Jr., J. E. Peralta, F. Ogliaro, M. J. Bearpark, J. J. Heyd, E. N. Brothers, K. N. Kudin, V. N. Staroverov, T. A. Keith, R. Kobayashi, J. Normand, K. Raghavachari, A. P. Rendell, J. C. Burant, S. S. Iyengar, J. Tomasi, M. Cossi, J. M. Millam, M. Klene, C. Adamo, R. Cammi, J. W. Ochterski, R. L. Martin, K. Morokuma, O. Farkas, J. B. Foresman and D. J. Fox, *Gaussian 16*, Gaussian, Inc. Wallingford, CT, 2016.